PROCEEDINGS OF SCIENCE

Muon-based Gamma/Proton Discrimination Study with LACT-KM2A Joint Observation

Yaling Chen,[a,*] **Hu Liu**[a,†] **and Min Jin**[a]

[a] *Southwest Jiaotong University,*
No. 999, Xi'an Road, Chengdu, 610031, Si Chuan,China

E-mail: huliu@swjtu.edu.cn

The Large Array of Imaging Atmospheric Cherenkov Telescopes (LACT) is an array of imaging atmospheric Cherenkov telescopes, while the Muon Detector (MD) of the square kilometer array (KM2A) measures the muon component of extensive air showers. Both are located at the LHAASO site. KM2A has demonstrated significant gamma/proton discrimination power, ranging from 10^2 to 10^5 at energies above several tens of TeV, particularly when the shower core is positioned within its boundaries. In the joint observations conducted by LACT and KM2A, LACT provides high resolution measurements of the core position and shower direction, especially for events where the core lies outside the KM2A area. This capability significantly extends the effective detection area and enhances angular resolution. The gamma/proton discrimination ability, as determined by the muon component detected by the MD for events with cores positioned outside the KM2A, is a crucial focus of this study. This work aims to explore the gamma/proton discrimination capability for events observed by both LACT and KM2A, showcasing the effective detection area and the associated gamma/proton discrimination capabilities.

39th International Cosmic Ray Conference (ICRC2025)
15–24 July 2025
Geneva, Switzerland

ICRC 2025
The Astroparticle Physics Conference
Geneva July 15-24, 2025

*Speaker

PoS(ICRC2025)700

1. Introduction

The quare kilometer array(KM2A) of Large High Altitude Air Shower Observatory (LHAASO) comprises 5195 electromagnetic particle detectors (ED) and 1188 muon detectors (MD), spanning an instrumented area of 1.3 km^2[1]. Crucially, the muon detector subsystem provides robust gamma/proton discrimination capability above tens TeV[2]. However, the angular resolution of KM2A is around 0.3 degree. On the other hand, imaging atmospheric Cherenkov telescopes (IACTs) – such as H.E.S.S.[3] and VERITAS[4] – achieve superior angular resolution(less than 0.1 degree). Similarly, the Large Array of Imaging Atmospheric Cherenkov Telescope (LACT) is composed of 32 imaging atmospheric Cherenkov telescopes located at LHAASO site, which deliver superior angular resolution[5]. Compared to the KM2A array, LACT offers a larger effective detection area and IACTs exhibits strong gamma/hadron discrimination capabilities, particularly in the energy range below several tens of TeV. By combining observations from the LACT telescope array and the KM2A array, the two systems exhibit complementary advantages: LACT provides a large effective area and high angular resolution, while KM2A offers enhanced gamma-ray and proton discrimination capability. This synergistic approach significantly improves sensitivity and accuracy in high-energy gamma-ray sources within the framework of high-energy astrophysics[6].

This article primarily investigates the gamma/proton discrimination capability of the muon detector (MD) observed by the LACT array under two scenarios: when the shower core is located inside versus outside the KM2A array. The study is structured into three main sections. Section 2 describes the simulation framework, including the detailed configurations for generating simulated data and the reconstruction methods for shower core position and arrival direction. Section 3 presents the principal results, covering the detection efficiency, effective area, and gamma/proton separation capability. Finally, Section 4 provides a comprehensive discussion and summary of the findings and performance expectations for IACT discrimination capabilities.

2. Simulation and method

Figure 1 outlines the full simulation workflow of this study. The process begins with detailed air shower simulations using CORSIKA(version v7.6400)[7], which generates comprehensive output data including both secondary particle datas and Cherenkov photons. These outputs are then processed through parallel simulation chains: the particle data is subjected to a precise detector response simulation for the KM2A array using the Geant4 toolkit[8], while simultaneously, the Cherenkov photon component is handled through dedicated telescope simulations employing the sim_telarray package [9]. Following the telescope simulations, advanced reconstruction algorithms are applied to reconstruct the primary gamma-ray direction and shower core position. The subsequent data integration phase involves careful matching of the two datasets through stringent consistency checks on both event numbering and true core positions. Crucially, this matching procedure incorporates the telescope-reconstructed core positions and arrival directions as inputs to the KM2A simulation chain, enabling robust reconstruction of the muon lateral distribution.

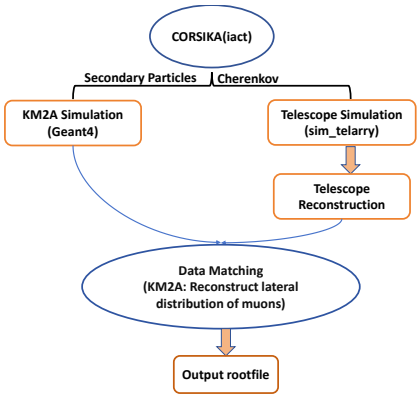

Figure 1: Simulation Workflow

2.1 Simulation

Using the CORSIKA software(version v7.6400)[7], we simulated the development of extensive air showers (EAS) in the atmosphere. The simulations were performed for two primary particle types: gamma rays and protons, spanning an energy range from 400 GeV to 400 TeV. All showers were generated with a zenith angle of 20° and an azimuthal angle of 0°, corresponding to the telescopes' pointing direction aligned with the primary particle arrival axis. The detector configuration was placed at an altitude of 4400 meters above sea level, with shower cores randomly distributed within a circular area of 1.3 km radius centered on the observation site.

Figure 2 illustrates a reconstructed proton event inside the KM2A array boundary. The black pentagram marks the ground truth shower core position, while the blue circles indicate reconstructed core positions. green triangles represent the geographical layout of LACT telescopes. In Figure 2a, the red pentagram denotes triggered electromagnetic detectors (EDs), whereas Figure 2b shows triggered muon detectors (MDs) with corresponding markers. Figure 2c displays the Cherenkov image from a triggered telescope after image cleaning. The black line represents the fit of the image. This visualization demonstrates the spatial correlation between the true event, reconstructed event, and detector responses.

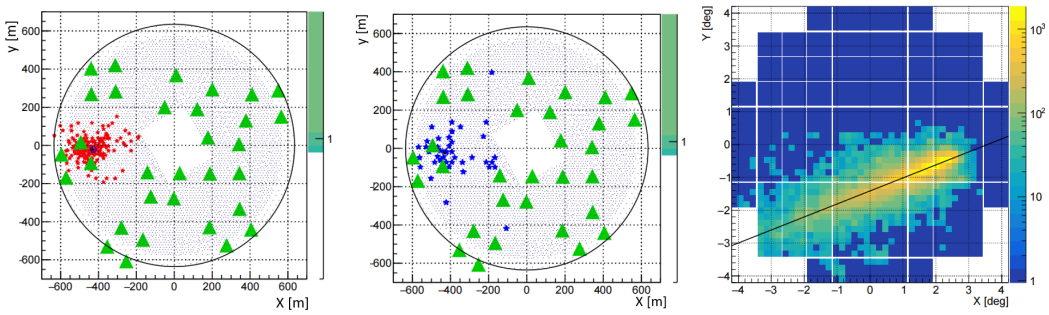

(a) trigger ED **(b)** trigger MD **(c)** The image of one trigger telescope of the 32 telescopes

Figure 2: The image of KM2A detectors and one triggered telescope

2.2 Core reconstruction and direction reconstruction

After simulating the telescope response, the recorded Cherenkov images are processed through the following sequential steps. First, a noise suppression algorithm is applied with a 10 photoelectron (p.e.) threshold to isolate significant pixel signals. The cleaned images are then analyzed to reconstruct the primary particle's arrival direction. For each cleaned image, Hillas parameters[10] are computed, including integrated photoelectron count across all pixels(A), x and y positions of the image centroid, angular distance between the centroid and the shower direction(φ), the length(L) and width(W) of the image. As shown in Figure 3, for every pair of telescopes, the direction of the primary particle and the position of the shower core can be determined. The intersecting line of the two telescopes' Shower Detector Planes defines the reconstructed shower axis (red line in the figure 3). The intersection point of this reconstructed shower axis with the ground gives the reconstructed core position (indicated by the black star in the figure 3). These individual estimates are subsequently combined through a weighted averaging method , yielding the final reconstructed shower core position and arrival direction. The weighting formula is a commonly adopted empirical expression, defined as:

$$w_{ij} = A_{\text{red}}^2 \sin^2(\varphi_i - \varphi_j)\delta_i^2\delta_j^2 \tag{1}$$

[11], where $A_{\text{red}} = \frac{A_i A_j}{A_i + A_j}$. In the analysis, A_i and A_j are the total photoelectron (p.e.) counts for the i-th and j-th telescopes, respectively. Parameters δ_i and δ_j are defined as $\delta = 1 - W/L$ for each telescope. Quantities φ_i and φ_j are the angular distances between the reconstructed shower centroid and true shower direction for the i-th and j-th telescopes.

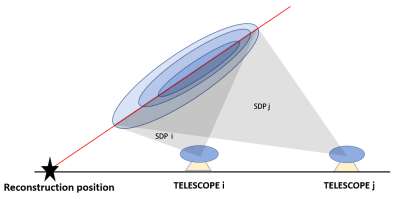

Figure 3: The method of reconstruct event

3. Result

3.1 Detection Efficiency

The detection efficiency of the telescope array is defined as:$\varepsilon = N_{\text{sel}}/N_{\text{all}}$, where ε represents detection efficiency of the telescope array, N_{all} denotes the number of simulated events within a given core position range, and N_{sel} represents the number of events retained after detectors trigger and event selection. Figure 4 illustrates the impact of energy and shower core position on the detection efficiency. The minimum distance between the shower core position and the KM2A array boundary is denoted as D. We set the energies to $10^{0.5}$ TeV, 10 TeV, $10^{1.5}$ TeV, $10^{2.0}$ TeV, and $10^{2.5}$ TeV, and the core positions to -300 m, -200 m, -110 m, -50 m, 0 m, 50 m, 100 m, and 150 m relative to the array boundary. When D is 0m, it indicates that the shower core position is located

on the array boundary; when D is positive, it indicates that the shower core position is located inside the array; and when D is negative, it indicates that the shower core position is located outside the array. As shown in Figure 4a, the detection efficiency of the telescope array versus distance D exhibits different trends at various energies. When the energy is fixed at $10^{2.5}$ TeV, full efficiency is maintained even at a core position 100 m outside the array boundary. Figure 4b shows the variation of detection efficiency with energy across different core position ranges. For a fixed core position range, the detection efficiency progressively increases with rising energy.

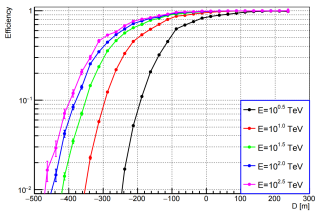

(a) Variation of detection efficiency with D at different energies.

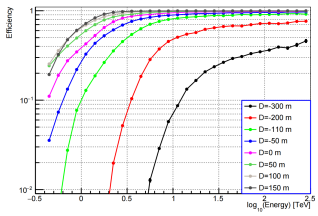

(b) variation of detection efficiency with D at fixed shower core positions

Figure 4: Detection efficiency vs. energy and core position

3.2 Effective area

The effective area serves as a crucial metric for characterizing the detection capability of the telescope array, defined mathematically as:Effective Area $= \int \varepsilon \times dS$, where the integration extends from the interior to the exterior boundary of the KM2A array, and ε denotes the position-dependent detection efficiency. Both the effective area and detection efficiency of the telescope array depend on energy. As illustrated in the figure 5, the effective area increases with rising energy. At approximately 10 TeV and the zenith angle of 20°, the effective area reaches $2 \times 10^6 m^2$ – significantly larger than that achieved by the KM2A array alone during standalone observations. Joint observations utilizing both the telescope array and KM2A array effectively compensate for the limited detection area of the KM2A.

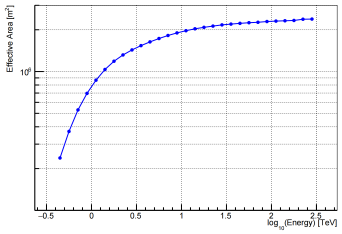

Figure 5: Effective area vs. energy

3.3 Gamma/Proton discrimination

3.3.1 Discriminant variable

This study employs muon information for gamma/proton discrimination to evaluate both the particle separation capability within the array boundary and the maximum effective distance beyond

the array boundary. Key discrimination variables include muon counts within annular radii of 15–200 m(denoted as $N_\mu(r < 200m)$ hereafter), 15–400 m(denoted as $N_\mu(r < 400m)$ hereafter), and 15–1500 m(denoted as $N_\mu(r < 1500m)$ hereafter), the total muon number derived from lateral distribution function fitting(denoted as N^{μ}_{size} hereafter), and muon density at r = 150 m(denoted as ρ^{μ}_{150} hereafter). The lateral distribution function is defined as

$$\rho(r) = N_{size}\, C(s) \left(\frac{r}{r_0}\right)^{s-2} \left(1 + \frac{r}{r_0}\right)^{(s+\Delta)} \tag{2}$$

where C(s) defines as $C(s) = \frac{1}{2\pi r_0} \cdot \frac{\Gamma(-s-\Delta)}{\Gamma(s)\Gamma(-\Delta-2s)}$, N_{size} denotes the total secondary particles, r is the perpendicular distance from the shower axis, s represents the shower age parameter, and r_0 is fixed at 800 m[12]. By treating N_{size} and s as free parameters, we compute $\rho(r)$ at discrete radial distances and obtain the total muon number through numerical integration over the domain. Figure 6 and Figure 7 show the variables as a function of the D for gamma and protons. Here, the distributions at 10^{-2} and 10^{-6} in the figure correspond to the fraction of events that do not produce muons.

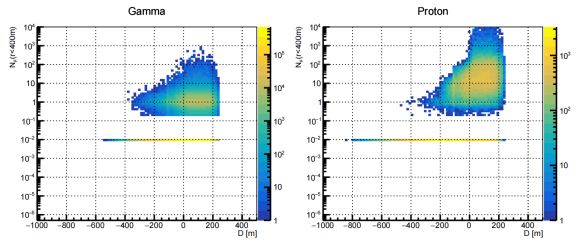

Figure 6: Distribution of $N_\mu(r < 400m)$

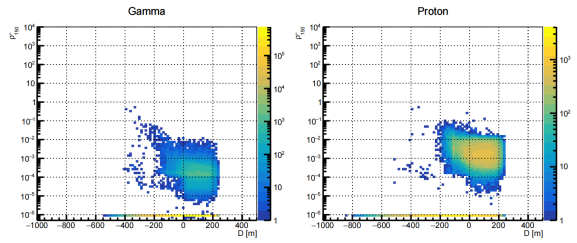

Figure 7: Distribution of ρ^{μ}_{150}

3.3.2 Discrimination power

Figure 8 displays the variation of proton rejection power with core distance D at fixed 90% of gamma efficiency, using the discrimination variables. The analysis is performed at energies of $10^{1.0}$ TeV, $10^{1.5}$ TeV, $10^{2.0}$ TeV, and $10^{2.5}$ TeV. In this analysis, we impose strict selection criteria on shower core positions. To achieve a proton rejection power of 10^2, the muon information detected by the muon detectors (MD) array exhibits effectively no discrimination capability at 10 TeV, as demonstrated in Figure 8a. At $10^{1.5}$ TeV, the discrimination capability remains substantially limited, with only $N_\mu(r < 400m)$ achieving a proton rejection power of 10^2 inside the array

boundary while exhibiting no effective discrimination beyond it. When energy increases to 100 TeV, the proton rejection power can reach 10^2 at approximately 60 m outside the array. At higher energies ($10^{2.5}$ TeV), this effective discrimination range extends to about 100 m beyond the boundary while maintaining equivalent rejection power, demonstrating a positive correlation between energy and spatial coverage of gamma/proton separation.

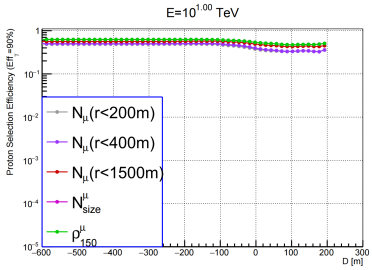

(a) The Proton rejection power at $10^{1.0}$TeV

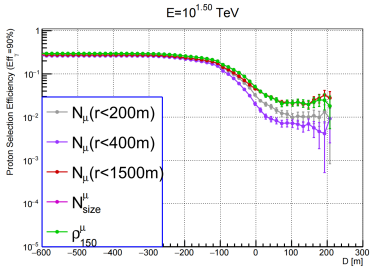

(b) The Proton rejection power at $10^{1.5}$TeV

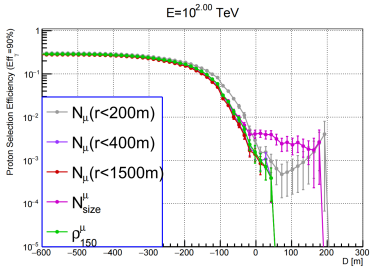

(c) The Proton rejection power at $10^{2.0}$TeV

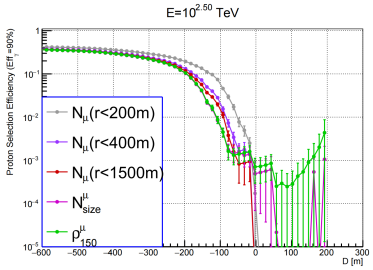

(d) The Proton rejection power at $10^{2.5}$TeV

Figure 8: Proton rejection power vs. core distance at different energies

4. Summary and outlook

This study primarily focuses on key performance parameters of the hybrid detector system combining the KM2A array and LACT telescope array. The KM2A array features an detection area of $1.3 \times 10^6 m^2$, while the integrated KM2A-LACT system achieves an effective area of $2 \times 10^6 m^2$ for gamma-ray observations – substantially larger than KM2A's detection area. Regarding gamma/proton discrimination using muon information from KM2A's Muon Detector (MD), a rejection power of 10^2 is attainable only within the array at $10^{1.5}$ TeV. This effective discrimination range extends with increasing energy, reaching up to 100 m beyond the array boundary while maintaining 10^2 of the proton rejection power at energy of $10^{2.5}$ TeV.

This work primarily provides the shower core position and direction reconstructed by the telescopes to KM2A for reconstruction. It currently demonstrates the discrimination capability using muon information as the distinguishing variable. Meanwhile, IACTs inherently possess strong gamma-hadron separation capabilities. Furthermore, the LACT array, composed of 32 IACTs, features good angular resolution and can also achieve effective gamma-hadron separation.

5. Acknowledgments

The work is supported by the National Natural Science Foundation of China (Grant number 12205244).

References

[1] Xin-Hua Ma, Yu-Jiang Bi, Zhen Cao, Ming-Jun Chen, Song-Zhan Chen, Yao-Dong Cheng, Guang-Hua Gong, Min-Hao Gu, Hui-Hai He, Chao Hou, et al. Lhaaso instruments and detector technology. *Chinese Physics C*, 46(3):030001, 2022.

[2] F Aharonian, Q An, LX Bai, YX Bai, YW Bao, D Bastieri, XJ Bi, YJ Bi, H Cai, JT Cai, et al. Observation of the crab nebula with lhaaso-km2a- a performance study. *Chinese Physics C*, 45(2):025002, 2021.

[3] K Bernlöhr. Hess—the high energy stereoscopic system. 2001.

[4] Nahee Park. Performance of the veritas experiment. *arXiv preprint arXiv:1508.07070*, 2015.

[5] SS Zhang, Yudong Wang, Jiali Liu, Shaohui Feng, Mingjie Yang, Lisi Genga, Yong Zhanga, et al. Large array of imaging atmospheric cherenkov telescopes (lact): status and future plans. In *Proceedings of 38th International Cosmic Ray Conference—PoS (ICRC2023)*, volume 444, page 808, 2024.

[6] Zhipeng Zhang, Ruizhi Yang, Shoushan Zhang, LiQiao Yin, Jiali Liu, Yudong Wang, Lingling Ma, and Zhen Cao. Prospects for joint reconstruction of imaging air cherenkov telescope array and extensive air shower array. *Journal of High Energy Astrophysics*, 43:280–285, 2024.

[7] Dieter Heck, Johannes Knapp, JN Capdevielle, G Schatz, T Thouw, et al. Corsika: A monte carlo code to simulate extensive air showers. *Report fzka*, 6019(11), 1998.

[8] Zhen Cao, F Aharonian, Q An, Axikegu, YX Bai, YW Bao, D Bastieri, XJ Bi, YJ Bi, JT Cai, et al. Lhaaso-km2a detector simulation using geant4. *Radiation Detection Technology and Methods*, 8(3):1437–1447, 2024.

[9] Konrad Bernlöhr. Corsika and sim_telarray–simulation of the imaging atmospheric cherenkov technique, 2001.

[10] A Michael Hillas. Cerenkov light images of eas produced by primary gamma. In *19th Intern. Cosmic Ray Conf-Vol. 3*, number OG-9.5-3, 1985.

[11] K Bernlöhr, A Barnacka, Yvonne Becherini, O Blanch Bigas, E Carmona, P Colin, G Decerprit, F Di Pierro, F Dubois, Christian Farnier, et al. Monte carlo design studies for the cherenkov telescope array. *Astroparticle Physics*, 43:171–188, 2013.

[12] Chen Yaling, Feng Zhang, Hu Liu, and Fengrong Zhu. Properties of secondary components in extensive air shower of cosmic rays in knee energy region. *arXiv preprint arXiv:2307.02068*, 2023.